THE JOURNAL OF PHYSICAL CHEMISTRY Letters

Letter

pubs.acs.org/JPCL

Composite Perovskites of Cesium Lead Bromide for Optimized Photoluminescence

Yichuan Ling,[†] Lei Tan,[†] Xi Wang,[†] Yan Zhou,[‡] Yan Xin,[∥] Biwu Ma,[§,⊥] Kenneth Hanson,[‡,⊥] and Hanwei Gao*[,†,∥,⊥]

[†]Department of Physics, [‡]Department of Chemistry and Biochemistry, [§]Department of Chemical and Biomedical Engineering, [∥]National High Magnetic Field Laboratory, and [⊥]Materials Science Program, Florida State University, Tallahassee, Florida 32306, United States

Supporting Information

ABSTRACT: The halide perovskite $CsPbBr_3$ has shown its promise for green light-emitting diodes. The optimal conditions of photoluminescence and the underlying photophysics, however, remain controversial. To address the inconsistency seen in the previous reports and to offer high-quality luminescent materials that can be readily integrated into functional devices with layered architecture, we created thin films of $CsPbBr_3/Cs_4PbBr_6$ composites based on a dual-source vapor-deposition method. With the capability of tuning the material composition in a broad range, $CsPbBr_3$ is identified as the only light emitter in the composites. Interestingly, the presence of the photoluminescence-inactive Cs_4PbBr_6 can significantly enhance the light emitting efficiency of the composites. The unique negative thermal quenching observed near the liquid nitrogen temperature indicates that a type of shallow state generated at the $CsPbBr_3/Cs_4PbBr_6$ interfaces is responsible for the enhancement of photoluminescence.

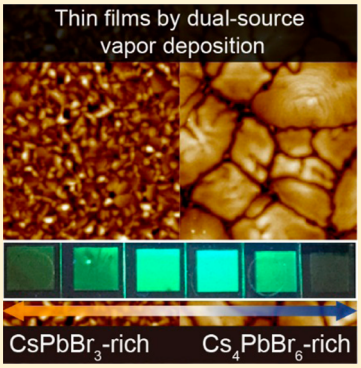

Halide perovskites have shown great potential as the building blocks for low-cost, high-performance optoelectronics.[1−7] Devices demonstrated successfully based on this class of materials include solar cells with efficiency exceeding 20%[5] and light emitting diodes (LEDs) with brightness comparable with commercial product.[2,8−10] Among the perovskites that exhibit remarkable photoresponse and charge transport properties, the ones without organic ions are particularly promising for being durable at elevated temperatures.[11−15] Such thermal stability is critical for applications like LEDs, which are often operated at higher voltage, and the local temperature from joule heating can be considerably high.

$CsPbBr_3$, an all-inorganic perovskite, has been used as the light emitter in green LEDs.[13,16−24] Although consistent photoluminescence (PL) and electroluminescence (EL) are observed from the direct bandgap transitions in $CsPbBr_3$, the mechanisms of the light emission remain controversial. For instance, the size of the $CsPbBr_3$ crystallites appears to be critical to the brightness of the photoluminescence. While the $CsPbBr_3$ powder can emit bright green light,[12,15] and isolated nanostructures of $CsPbBr_3$ can even lase under optical pump,[17,18] large single crystals of $CsPbBr_3$ exhibit much weaker PL.[25,26] Meanwhile, Cs_4PbBr_6 was also reported to emit bright green emission even though the bandgap is located in the UV spectral range.[27−30] These inconsistent observations have posed fundamental questions to the photophysics and restrained the development of high-efficiency $CsPbBr_3$-based LEDs.[31] In this work, we created $CsPbBr_3/Cs_4PbBr_6$ (CPB113/CPB416) composites for optimized photoluminescence using a vapor-deposition method. Compared with solution synthesis, the method based on dual-source thermal evaporation provides the flexibility to tuning the concentration of the component materials in a wide range, which is critical for understanding the luminescent behaviors in these composites. While CPB113 is identified as the only light emitter, the PL-inactive hexabromide CPB416 can enhance the PL processes by forming a host−guest system with the CPB113 crystallites and passivating the grain boundaries with a type of luminescent shallow states. The findings can be used to resolve the controversies and discrepancies seen in previous reports, and guide the design of composite perovskite materials for optimized light emission performance.

Solution synthesis of halide perovskites, although simple and cost-effective, is primarily governed by the thermodynamics.[32,33] Crystallites precipitating from precursor solutions are often in the energy-favorable phases with limited control over the composition, which makes it challenging, particularly when composites of multiple crystalline phases are being pursued.[12] In this work, instead, we prepared thin films of perovskite composites using a vapor deposition method (Figure 1a). Alternating layers of $PbBr_2$ and CsBr were first thermally evaporated onto glass substrates, followed by thermal annealing at 100 °C for thorough diffusion and reactions between the solid-state precursors. Flexible control over the quantities of the component elements evaporated (Table S1) leads to the highly tunable weight ratio between CPB113 and CPB416 in the

Received: May 24, 2017
Accepted: July 5, 2017
Published: July 5, 2017

DOI: 10.1021/acs.jpclett.7b01302
J. Phys. Chem. Lett. 2017, 8, 3266−3271

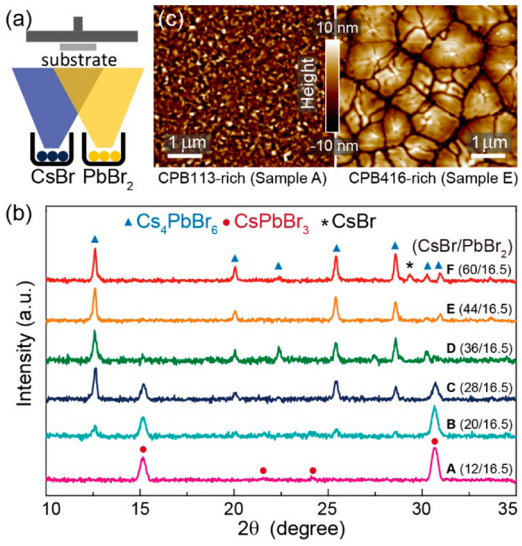

Figure 1. Thin films of perovskite composites have been obtained. (a) The schematics of the dual-source vapor deposition. (b) The XRD patterns of the perovskite composites. (c) AFM images of the $CsPbBr_3$-rich (left) and the Cs_4PbBr_6-rich (right) thin films.

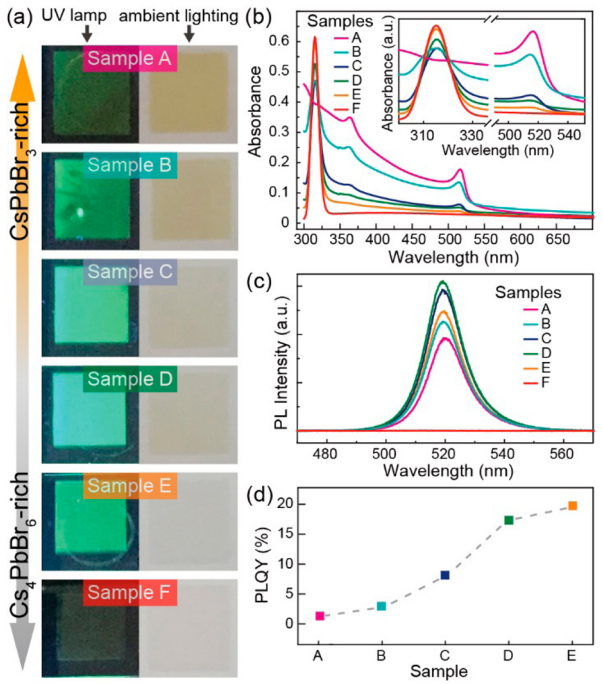

Figure 2. The presence of Cs_4PbBr_6 significantly affects the luminescent properties of the perovskite composites. (a) Thin films with various compositions under the 365 nm Hg lamp (left) and the ambient light (right). (b) The UV−vis absorbance, (c) PL spectra, and (d) PL quantum yield (PLQY) of the composites.

composite thin films obtained. X-ray diffraction (XRD) patterns show that Sample A contains nearly pure CPB113 and Sample F is predominately CPB416 (Figure 1b). In between, the more CsBr is deposited, the higher concentration of CPB416 is found in the annealed composites. It is worth noting that Sample F is made with excessive CsBr precursor (observable in the XRD pattern) in order to minimize the CPB113 contained in the annealed product. The composite films created using this method, regardless of the ratio between the two phases, exhibit low surface roughness and pinhole free morphology (Figure 1c). Creating high-quality thin films of Cs-based perovskites used to be challenging for solution synthesis; low solubility of Cs precursors (e.g., CsBr in the polar solvent) often leads to high surface roughness and unsatisfactory film coverage.[19,20]

The capability of preparing the CPB113/CPB416 composites with nominally arbitrary weight ratio allows us to identify the green light emitter between the two component phases. The thin film containing predominantly CPB416 (Sample F) exhibits negligible PL under the 365 nm Hg lamp, while all others emit green light (Figure 2a). The PL around 520 nm is located close to the absorption edge (Figure 2b,c). This absorption edge is distinct in the composites containing CPB113 and becomes lower in magnitude as the concentration of CPB113 decreases, which makes the samples more transparent under ambient light (Figure 2a). As the optical absorption in the visible range keeps decreasing from Sample A to F, the absorption in UV (around 316 nm) becomes stronger. In the extreme case where CPB113 is negligible (Sample F), the peak in UV becomes the only noticeable spectral feature in the absorption spectrum. The correlation between the PL and the absorption spectra indicates that only the CPB113 phase is responsible for the light emission around 520 nm, which originates from the excitonic recombination near the edges of the direct bandgap.[12,34,35] The CPB416 phase, alternatively, exhibits a bandgap at a UV wavelength (316 nm) and does not produce PL in the visible range (Figure S1).[36−38] For verification purposes, we deposited excessive CsBr precursor during the evaporation, which turns out necessary to eliminate trace amount of CPB113.[38] The thin film obtained in this manner (Sample F) exhibits the negligible PL intensity and the minimal absorbance in the visible range.

Interestingly, although being PL-inactive, the presence of CPB416 in the composites has significant effects on the PL enhancement. A higher concentration of CPB113 in the composites, with stronger absorption in the visible range, does not necessarily lead to stronger PL emission around 520 nm. In fact, as the quantity of CPB113 in the films decreases (which can be deduced from the absorbance), the PL intensity increases instead. By measuring the PL quantum yield (PLQY) using an integrating sphere, we found surprisingly that the efficiency of the PL increases when higher concentration of CPB416 is incorporated in the composite thin films (Figure 2d). Among the composites that contain a noticeable amount of CPB113, Sample E has the lowest quantity of CPB113 but exhibits the highest PL efficiency. Note that the CPB113 component can be barely identified in the XRD pattern of the highly luminescent Sample E, which means XRD is not sensitive enough to determine the small quantities of luminescent components that can be responsible for the light emission from the composite materials. This explains why powders, single-crystals, and nanocrystals dominated by CPB416 were sometimes considered luminescent by mistake previously.[12,34] Such increase of PLQY as a function of the composite concentration is similar to the optical properties of CPB113/CPB416 nanocrystals reported by Sargent and co-workers.[12] Differently, the PLQY of the solution synthesized composite nanocrystals (in ref 12) exhibits a maxima with an intermediate CPB113/CPB416 ratio, whereas PLQY of the coevaporated composite thin films in this work increases monotonically with higher concentration of CPB416. Such observation indicates that the material preparation methods could lead to different light emission behaviors, which is

DOI: 10.1021/acs.jpclett.7b01302
J. Phys. Chem. Lett. 2017, 8, 3266−3271

expected given that the interfacial states between the two phases are considered to contribute to the concentration-dependent PLQY (see further discussion below).

To understand the roles that CPB416 plays in enhancing the PL from CPB113, we examined and compared the microscopic morphology of the composite thin films that are dominated by CPB113 (Sample A), by CPB416 (Sample E), and with considerable quantities of both (Sample C), respectively. Transmission electron microscopy (TEM) images show two sizes of crystalline grains: the smaller grains (<150 nm) that dominate Sample A (Figure 3a) and the larger domains with

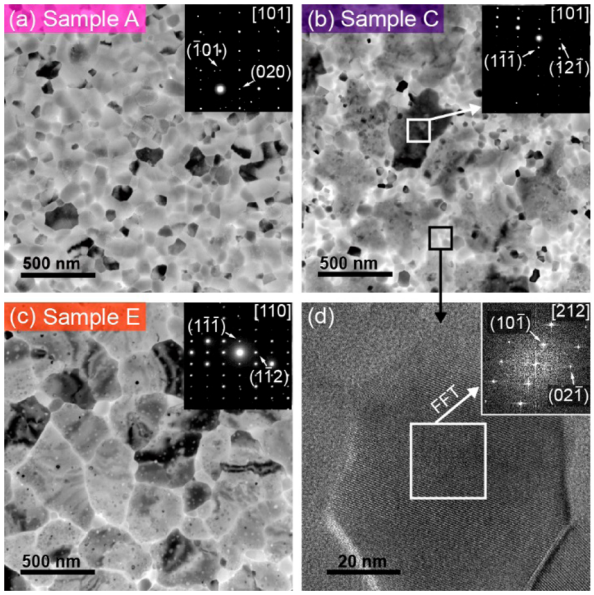

Figure 3. TEM images show the microscopic morphology of the perovskite composites. Bright-field TEM images from samples containing (a) purely CPB113, (b) a mixture of CPB113 and CPB416, and (c) predominantly CPB416. (d) High-resolution bright-field image from a small domain in Sample C and the corresponding fast Fourier transformed diffraction pattern.

irregular shapes that dominate Sample E (Figure 3c). Based on the material composition implied by the XRD patterns (Figure 1b) and the TEM electron diffraction patterns (Figure 3a–d, insets), the smaller domains can be determined to be CPB113 in the orthorhombic phase, whereas the larger ones are CPB416 with rhombohedral lattices. In Sample C, these two types of domains are mixed uniformly at the microscopic scale (Figure 3b). It is notable that the average size of the CPB113 domains in Sample C is smaller compared to that in Sample A. The reaction between $CsPbBr_3$ and residual CsBr during the postevaporation annealing can generate more CPB416 and reduce the size of the CPB113 domains. The small amount of CPB113 contained in Sample E, which is shown in the optical absorption and emission spectra, is not obvious in the microscopic images, which can be a combined result of minimal quantity of CPB113 and further reduced sizes of the CPB113 domains.

Temperature-dependent PL indicates that the enhanced PL in the perovskite composites may originate from passivated interfaces and increased exciton binding energy. As the temperature is lowered from 300 K, the integrated PL intensity first increases, followed by a decrease as the temperature further reduces (Figure 4). While more intense PL is typically expected

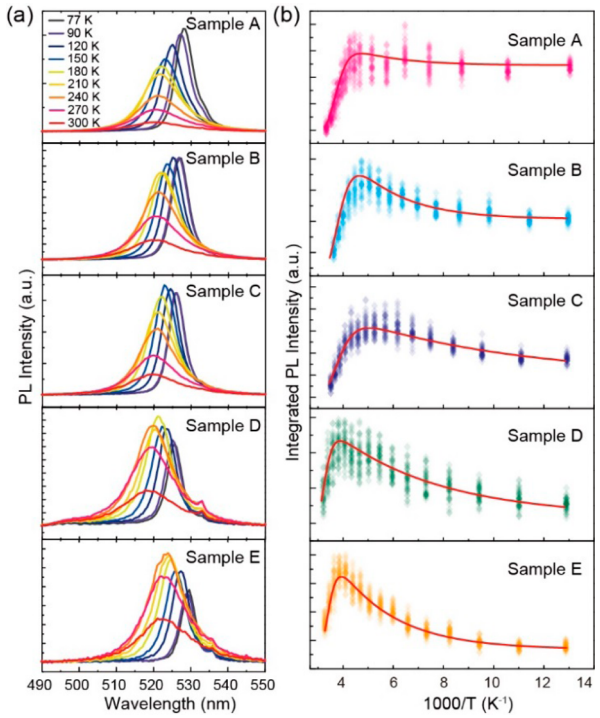

Figure 4. Temperature-dependent PL spectra indicate the mechanisms of the PL enhancement in the perovskite composites. (a) PL spectra collected from 77 K to room temperature (300 K). (b) Integrated PL intensity as the function of temperature. The solid curves are the fitting results based on the exciton-trap model. PL spectra were taken 50 times at each selected temperature for more reliable fitting. The fluctuations in the signal are primarily caused by the fluctuations from the q-switch laser source.

at lower temperatures due to the suppressed phonon-assisted nonradiative recombination,[21] a reduction in the PL intensity at lower temperatures is rarely observed. A mechanism that can lead to such so-called negative thermal quenching is the shallow trap states located near the edge of the bandgap.[39] The ionization energy of these states has to be so small that thermal perturbations (k_BT) at the room temperature are sufficient to excite the carriers trapped in these shallow states. These shallow states, therefore, are not effective traps at the room temperature. As the temperature reduces, k_BT decreases; the trapped carriers are less likely to be brought back thermally to the energy bands and, therefore, quench the PL.

The temperature-dependent PL of the perovskite composites can be fit well using a combined exciton-trap model:[39]

$$I(T) = I(0)\frac{1 + D_1 \exp\left(-\frac{E_q}{k_BT}\right)}{1 + C_1 \exp\left(-\frac{E_j}{k_BT}\right)} \quad (1)$$

E_j is the exciton binding energy, E_q is the ionization energy of the trap state, and $I(T)$ and $I(0)$ are the integrated PL intensities at a finite temperature and hypothetically 0 K, respectively. The fitting results (Table S2), with some fluctuation, show the following characteristics:

(i) The depth of the trap states E_q from all the five luminescent composites are comparable to k_BT at room temperature (~26 meV), consistent with the expectation of shallow trap states that can lead to the negative thermal quenching observed.

DOI: 10.1021/acs.jpclett.7b01302
J. Phys. Chem. Lett. 2017, 8, 3266–3271

(ii) The coefficient D_1, associated with the shallow traps, increases as the concentration of CPB416 becomes higher, indicating that the more CPB416 is contained, the more these shallow trap states are created. To participate in producing PL at room temperature, these trap states have to be associated with the PL-active component, CPB113, in the perovskite composites, either at the surface or in the bulk of the CPB113 domains. Given the morphology the CPB416/CPB113 composites revealed by the TEM images, we speculate that the increased density of the shallow trap states is associated with the interfaces between the CPB416 and CPB113 domains. Essentially, the incorporation of CPB416 passivates the surface of CPB113 domains with shallow interfacial traps. As shown in Figure 5a, after photoexcitation, part of the photoexcited electron in the conduction band can be trapped in these shallow traps. At room temperature, these trapped electrons can be thermally ionized followed by the formation of radiative excitons. These shallow traps, therefore, essentially participate in the photoluminescence processes and can be considered to be in the bright state (PL active). Alternatively, when the temperature is sufficiently low, the thermal perturbation (k_BT) is not enough to bring the trapped electrons to the conduction band. Those trapped carriers will decay through nonradiative pathways, leading to the observed negative thermal quenching (i.e., weaker PL at lower temperature). This model explains why the more the CPB416 are present, the higher PL efficiency is obtained and why more significant PL quenching is observed at low temperatures.

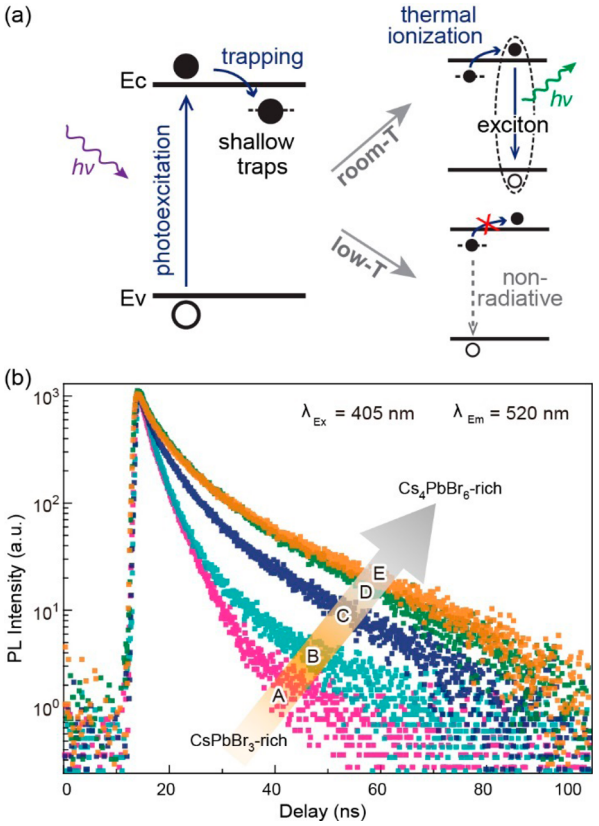

Figure 5. (a) Schematics of the shallow traps which lead to the observed negative thermal quenching. (b) The enhanced PL at the room temperature is accompanied by longer PL lifetimes.

(iii) Larger exciton binding energy E_j is observed with higher concentration of CPB416. As discussed earlier, when more CPB416 is incorporated in the composites, the domain size of the CPB113 crystallites becomes smaller. The reduction in the dimension of CPB113 crystallites is also evident from the blue-shifted PL (Figure S2). Stronger Coulomb interactions (between the excited charge carriers) from the spatial confinement can increase the exciton binding energy, which in principle can enhance the PL efficiency. The fitting results, however, show that the exciton binding energy in all of the samples is on the order of hundreds of meV, significantly larger than the k_BT at room temperature. The effects of increased binding energy, therefore, should not be the major factor for the enhanced PL observed in these composites.

The enhanced PL from the CPB416-rich composites is accompanied by longer PL lifetime (Figure 5). All the time-dependent PL traces can be fit well using a double exponential function:

$$R(t) = B_1 e^{(-t/\tau_1)} + B_2 e^{(-t/\tau_2)} \quad (2)$$

The fast component τ_1 is typically attributed to the surface trapping, and the slow component τ_2 is considered the lifetime of radiative recombination.[40] While τ_1 approaches the temporal resolution limit of the nanosecond transient spectroscopy and may not be accurately determined, significant increase in τ_2 can be observed in the composites containing higher concentration of CPB416 (Table S3). This phenomenon can be attributed to the thermal ionization of the shallow trap states, which contributes to the PL at room temperature and increases the combined lifetime of the radiative recombination processes. Together with the correlation between the PL efficiency and the material composition, it can be determined that larger amount of CPB416 leads to the suppression of the fast nonradiative process. This is consistent with results from the temperature dependent PL measurements, which indicate that the incorporation of CPB416 passivates the surfaces of CPB113 domains with shallow trap states that are PL-active and can enhance the PL efficiency at room temperature.

In conclusion, we developed a facile approach to grow composite thin films of all-inorganic halide perovskites. The flexible control of the material composition provides a platform to uncover the optimal conditions for light emission from the $CsPbBr_3$ perovskite. The PL-inactive component, CPB416, is found to be critical in enhancing the PL efficiency of the luminescent CPB113 crystallites. A type of shallow trap states, which has not been observed previously in halide perovskites, is formed likely at the CPB416/CPB113 grain boundaries and is responsible for the PL enhancement observed. While previous work on halide perovskites pursued exclusively homogeneous materials, our results show that composites with deliberately designed heterogeneous interfaces offer new opportunities for studying and optimizing the material properties and functionalities, and thus should be included into considerations in the future design of the optoelectronic halide perovskites.

DOI: 10.1021/acs.jpclett.7b01302
J. Phys. Chem. Lett. 2017, 8, 3266−3271

■ ASSOCIATED CONTENT

Supporting Information

The Supporting Information is available free of charge on the ACS Publications website at DOI: 10.1021/acs.jpclett.7b01302.

Experimental methods, addition PL spectra, and fitting results of time-dependent and temperature-dependent PL measurements (PDF)

■ AUTHOR INFORMATION

Corresponding Author

*E-mail: hgao3@fsu.edu.

ORCID

Biwu Ma: 0000-0003-1573-8019

Kenneth Hanson: 0000-0001-7219-7808

Hanwei Gao: 0000-0001-8085-8178

Author Contributions

The manuscript was written through contributions of all authors. All authors have given approval to the final version of the manuscript.

Notes

The authors declare no competing financial interest.

■ ACKNOWLEDGMENTS

This work made use of the Condensed Matter and Material Physics Facility, the MAC Laboratory, and the Electron Microscopy Center at Florida State University. The temperature-dependent PL measurements were performed on a transient absorption spectrometer acquired with the support from the National Science Foundation (Grant No. CHE-1531629). The authors thank Dr. Eric Lochner and Dr. Bert van de Burgt for the help with optical and microscopic measurements. This work is financially supported by Florida State University through the Energy and Materials Initiative.

■ REFERENCES

(1) Saparov, B.; Mitzi, D. B. Organic-Inorganic Perovskites: Structural Versatility for Functional Materials Design. *Chem. Rev.* **2016**, *116*, 4558−4596.

(2) Xiao, Z.; Kerner, R. A.; Zhao, L.; Tran, N. L.; Lee, K. M.; Koh, T.-W.; Scholes, G. D.; Rand, B. P. Efficient Perovskite Light-Emitting Diodes Featuring Nanometre-Sized Crystallites. *Nat. Photonics* **2017**, *11*, 108−115.

(3) Cho, H.; Jeong, S.-H.; Park, M.-H.; Kim, Y.-H.; Wolf, C.; Lee, C.-L.; Heo, J. H.; Sadhanala, A.; Myoung, N.; Yoo, S.; et al. Overcoming the Electroluminescence Efficiency Limitations of Perovskite Light-Emitting Diodes. *Science* **2015**, *350*, 1222−1225.

(4) Docampo, P.; Bein, T. A Long-Term View on Perovskite Optoelectronics. *Acc. Chem. Res.* **2016**, *49*, 339−346.

(5) Yang, W. S.; Noh, J. H.; Jeon, N. J.; Kim, Y. C.; Ryu, S.; Seo, J.; Seok, S. I. High-Performance Photovoltaic Perovskite Layers Fabricated through Intramolecular Exchange. *Science* **2015**, *348*, 1234−1237.

(6) Zhao, Y.; Zhu, K. Organic-Inorganic Hybrid Lead Halide Perovskites for Optoelectronic and Electronic Applications. *Chem. Soc. Rev.* **2016**, *45*, 655−689.

(7) Chen, Q.; De Marco, N.; Yang, Y.; Song, T.-B.; Chen, C.-C.; Zhao, H.; Hong, Z.; Zhou, H.; Yang, Y. Under the Spotlight: The Organic-Inorganic Hybrid Halide Perovskite for Optoelectronic Applications. *Nano Today* **2016**, *10*, 355−396.

(8) Ling, Y.; Tian, Y.; Wang, X.; Wang, J. C.; Knox, J. M.; Perez-Orive, F.; Du, Y.; Tan, L.; Hanson, K.; Ma, B.; et al. Enhanced Optical and Electrical Properties of Polymer-Assisted All-Inorganic Perovskites for Light-Emitting Diodes. *Adv. Mater.* **2016**, *28*, 8983−8989.

(9) Qian, L.; Zheng, Y.; Xue, J.; Holloway, P. H. Stable and Efficient Quantum-Dot Light-Emitting Diodes Based on Solution-Processed Multilayer Structures. *Nat. Photonics* **2011**, *5*, 543−548.

(10) Li, J.; Shan, X.; Bade, S. G. R.; Geske, T.; Jiang, Q.; Yang, X.; Yu, Z. Single-Layer Halide Perovskite Light-Emitting Diodes with Sub-Band Gap Turn-On Voltage and High Brightness. *J. Phys. Chem. Lett.* **2016**, *7*, 4059−4066.

(11) Berry, J.; Buonassisi, T.; Egger, D. A.; Hodes, G.; Kronik, L.; Loo, Y.-L.; Lubomirsky, I.; Marder, S. R.; Mastai, Y.; Miller, J. S.; et al. Hybrid Organic−Inorganic Perovskites (HOIPs): Opportunities and Challenges. *Adv. Mater.* **2015**, *27*, 5102−5112.

(12) Quan, L. N.; Quintero-Bermudez, R.; Voznyy, O.; Walters, G.; Jain, A.; Fan, J. Z.; Zheng, X.; Yang, Z.; Sargent, E. H. Highly Emissive Green Perovskite Nanocrystals in a Solid State Crystalline Matrix. *Adv. Mater.* **2017**, *29*, 1605945.

(13) Beal, R. E.; Slotcavage, D. J.; Leijtens, T.; Bowring, A. R.; Belisle, R. A.; Nguyen, W. H.; Burkhard, G. F.; Hoke, E. T.; McGehee, M. D. Cesium Lead Halide Perovskites with Improved Stability for Tandem Solar Cells. *J. Phys. Chem. Lett.* **2016**, *7*, 746−751.

(14) Saliba, M.; Matsui, T.; Seo, J.-Y.; Domanski, K.; Correa-Baena, J.-P.; Nazeeruddin, M. K.; Zakeeruddin, S. M.; Tress, W.; Abate, A.; Hagfeldt, A.; et al. Cesium-Containing Triple Cation Perovskite Solar Cells: Improved Stability, Reproducibility and High Efficiency. *Energy Environ. Sci.* **2016**, *9*, 1989−1997.

(15) Wang, Y.; Li, X.; Song, J.; Xiao, L.; Zeng, H.; Sun, H. All-Inorganic Colloidal Perovskite Quantum Dots: A New Class of Lasing Materials with Favorable Characteristics. *Adv. Mater.* **2015**, *27*, 7101−7108.

(16) Zhang, D.; Eaton, S. W.; Yu, Y.; Dou, L.; Yang, P. Solution-Phase Synthesis of Cesium Lead Halide Perovskite Nanowires. *J. Am. Chem. Soc.* **2015**, *137*, 9230−9233.

(17) Eaton, S. W.; Lai, M.; Gibson, N. A.; Wong, A. B.; Dou, L.; Ma, J.; Wang, L.-W.; Leone, S. R.; Yang, P. Lasing in Robust Cesium Lead Halide Perovskite Nanowires. *Proc. Natl. Acad. Sci. U. S. A.* **2016**, *113*, 1993−1998.

(18) Fu, Y.; Zhu, H.; Stoumpos, C. C.; Ding, Q.; Wang, J.; Kanatzidis, M. G.; Zhu, X.; Jin, S. Broad Wavelength Tunable Robust Lasing from Single-Crystal Nanowires of Cesium Lead Halide Perovskites ($CsPbX_3$, X = Cl, Br, I). *ACS Nano* **2016**, *10*, 7963−7972.

(19) Yantara, N.; Bhaumik, S.; Yan, F.; Sabba, D.; Dewi, H. A.; Mathews, N.; Boix, P. P.; Demir, H. V.; Mhaisalkar, S. Inorganic Halide Perovskites for Efficient Light-Emitting Diodes. *J. Phys. Chem. Lett.* **2015**, *6*, 4360−4364.

(20) Wei, Z.; Perumal, A.; Su, R.; Sushant, S.; Xing, J.; Zhang, Q.; Tan, S. T.; Demir, H. V.; Xiong, Q. Solution-Processed Highly Bright and Durable Cesium Lead Halide Perovskite Light-Emitting Diodes. *Nanoscale* **2016**, *8*, 18021−18026.

(21) Li, X.; Wu, Y.; Zhang, S.; Cai, B.; Gu, Y.; Song, J.; Zeng, H. $CsPbX_3$ Quantum Dots for Lighting and Displays: Room-Temperature Synthesis, Photoluminescence Superiorities, Underlying Origins and White Light-Emitting Diodes. *Adv. Funct. Mater.* **2016**, *26*, 2435−2445.

(22) Zhang, X.; Lin, H.; Huang, H.; Reckmeier, C.; Zhang, Y.; Choy, W. C. H.; Rogach, A. L. Enhancing the Brightness of Cesium Lead Halide Perovskite Nanocrystal Based Green Light-Emitting Devices through the Interface Engineering with Perfluorinated Ionomer. *Nano Lett.* **2016**, *16*, 1415−1420.

(23) Bade, S. G. R.; Li, J.; Shan, X.; Ling, Y.; Tian, Y.; Dilbeck, T.; Besara, T.; Geske, T.; Gao, H.; Ma, B.; et al. Fully Printed Halide Perovskite Light-Emitting Diodes with Silver Nanowire Electrodes. *ACS Nano* **2016**, *10*, 1795−1801.

(24) Song, J.; Li, J.; Li, X.; Xu, L.; Dong, Y.; Zeng, H. Quantum Dot Light-Emitting Diodes Based on Inorganic Perovskite Cesium Lead Halides ($CsPbX_3$). *Adv. Mater.* **2015**, *27*, 7162−7167.

(25) Rakita, Y.; Kedem, N.; Gupta, S.; Sadhanala, A.; Kalchenko, V.; Böhm, M. L.; Kulbak, M.; Friend, R. H.; Cahen, D.; Hodes, G. Low-Temperature Solution-Grown $CsPbBr_3$ Single Crystals and Their Characterization. *Cryst. Growth Des.* **2016**, *16*, 5717−5725.

DOI: 10.1021/acs.jpclett.7b01302
J. Phys. Chem. Lett. 2017, 8, 3266−3271

(26) Stoumpos, C. C.; Malliakas, C. D.; Peters, J. A.; Liu, Z.; Sebastian, M.; Im, J.; Chasapis, T. C.; Wibowo, A. C.; Chung, D. Y.; Freeman, A. J.; et al. Crystal Growth of the Perovskite Semiconductor $CsPbBr_3$: A New Material for High-Energy Radiation Detection. *Cryst. Growth Des.* **2013**, *13*, 2722−2727.
(27) Saidaminov, M. I.; Almutlaq, J.; Sarmah, S.; Dursun, I.; Zhumekenov, A. A.; Begum, R.; Pan, J.; Cho, N.; Mohammed, O. F.; Bakr, O. M. Pure Cs_4PbBr_6: Highly Luminescent Zero-Dimensional Perovskite Solids. *ACS Energy Lett.* **2016**, *1*, 840−845.
(28) Chen, D.; Wan, Z.; Chen, X.; Yuan, Y.; Zhong, J. Large-Scale Room-Temperature Synthesis and Optical Properties of Perovskite-Related Cs_4PbBr_6 Fluorophores. *J. Mater. Chem. C* **2016**, *4*, 10646−10653.
(29) Zhang, Y.; Saidaminov, M. I.; Dursun, I.; Yang, H.; Murali, B.; Alarousu, E.; Yengel, E.; Alshankiti, B. A.; Bakr, O. M.; Mohammed, O. F. Zero-Dimensional Cs_4PbBr_6 Perovskite Nanocrystals. *J. Phys. Chem. Lett.* **2017**, *8*, 961−965.
(30) Cha, J.-H.; Han, J. H.; Yin, W.; Park, C.; Park, Y.; Ahn, T. K.; Cho, J. H.; Jung, D.-Y. Photoresponse of $CsPbBr_3$ and Cs_4PbBr_6 Perovskite Single Crystals. *J. Phys. Chem. Lett.* **2017**, *8*, 565−570.
(31) Li, X.; Cao, F.; Yu, D.; Chen, J.; Sun, Z.; Shen, Y.; Zhu, Y.; Wang, L.; Wei, Y.; Wu, Y.; et al. All Inorganic Halide Perovskites Nanosystem: Synthesis, Structural Features, Optical Properties and Optoelectronic Applications. *Small* **2017**, *13*, 1603996.
(32) Kerner, R. A.; Zhao, L.; Xiao, Z.; Rand, B. P. Ultrasmooth Metal Halide Perovskite Thin Films via Sol-Gel Processing. *J. Mater. Chem. A* **2016**, *4*, 8308−8315.
(33) Yan, K.; Long, M.; Zhang, T.; Wei, Z.; Chen, H.; Yang, S.; Xu, J. Hybrid Halide Perovskite Solar Cell Precursors: Colloidal Chemistry and Coordination Engineering Behind Device Processing for High Efficiency. *J. Am. Chem. Soc.* **2015**, *137*, 4460−4468.
(34) Akkerman, Q. A.; Park, S.; Radicchi, E.; Nunzi, F.; Mosconi, E.; De Angelis, F.; Brescia, R.; Rastogi, P.; Prato, M.; Manna, L. Nearly Monodisperse Insulator Cs_4PbX_6 (X = Cl, Br, I) Nanocrystals, Their Mixed Halide Compositions, and Their Transformation into CsPbX3 Nanocrystals. *Nano Lett.* **2017**, *17*, 1924−1930.
(35) Kondo, S.; Kakuchi, M.; Masaki, A.; Saito, T. Strongly Enhanced Free-Exciton Luminescence in Microcrystalline $CsPbBr_3$ Films. *J. Phys. Soc. Jpn.* **2003**, *72*, 1789−1791.
(36) Nikl, M.; Mihokova, E.; Nitsch, K.; Somma, F.; Giampaolo, C.; Pazzi, G. P.; Fabeni, P.; Zazubovich, S. Photoluminescence of Cs_4PbBr_6 Crystals and Thin Films. *Chem. Phys. Lett.* **1999**, *306*, 280−284.
(37) Kondo, S.; Amaya, K.; Saito, T. Amorphous $CsPbX_3$ versus Crystalline Cs_4PbX_6 (X= Br, Cl)-Their Localized Electronic States Studied by Optical Absorption Spectroscopy. *J. Phys. Soc. Jpn.* **2001**, *70*, 3751−3752.
(38) Kondo, S.; Amaya, K.; Saito, T. Localized Optical Absorption in Cs_4PbBr_6. *J. Phys.: Condens. Matter* **2002**, *14*, 2093.
(39) Shibata, H. Negative Thermal Quenching Curves in Photoluminescence of Solids. *Jpn. J. Appl. Phys.* **1998**, *37*, 550.
(40) Shi, D.; Adinolfi, V.; Comin, R.; Yuan, M.; Alarousu, E.; Buin, A.; Chen, Y.; Hoogland, S.; Rothenberger, A.; Katsiev, K.; et al. Low Trap-State Density and Long Carrier Diffusion in Organolead Trihalide Perovskite Single Crystals. *Science* **2015**, *347*, 519−522.

DOI: 10.1021/acs.jpclett.7b01302
J. Phys. Chem. Lett. 2017, 8, 3266−3271